



# Optimization and fabrication of curvilinear micro-grooved cutting tools for sustainable machining based on finite element modelling of the cutting process

Guoliang Liu<sup>1</sup> · Tuğrul Özel<sup>2</sup> · Jianming Li<sup>3</sup> · Dexiang Wang<sup>1</sup> · Shufeng Sun<sup>1</sup>

Received: 28 April 2020 / Accepted: 9 August 2020 / Published online: 23 August 2020  
© Springer-Verlag London Ltd., part of Springer Nature 2020

## Abstract

The benefits of micro-textures on cutting tools have been confirmed widely in implementing sustainable machining. However, the derivative cutting processes induced by the sharp edges of textures weakened the potential benefits. In our preliminary work, the newly designed curvilinear micro-grooved cutting tool has been proved to eliminate derivative cutting processes and implement sustainable machining than non-textured tools by three-dimensional (3D) finite element (FE) simulations. In this paper, the curvilinear micro-groove structures were optimized and fabricated to further improve the cutting performance of minimizing specific cutting energy. The results indicated that all the micro-groove parameters, including the width, spacing, depth, and edge distance (the distance from cutting edge to the micro-grooved area), showed obvious influence on specific cutting energy in their own ways. Specific cutting energy of the metal cutting processes can be effectively reduced by the optimal curvilinear micro-grooved cutting tools, although the optimal structures used in rough and finish turning conditions were different. In addition, a new two-step method was developed in this work to prepare curvilinear micro-grooves on carbide tools with femtosecond laser. The optimal curvilinear micro-grooved cutting tools were fabricated and used in cutting experiments, which verified the simulative results.

**Keywords** Sustainable machining · Curvilinear micro-grooves · Specific cutting energy · Femtosecond laser processing · FEM

## 1 Introduction

In modern days, sustainable machining has been the most important trend in machining industrial fields. Adopting sustainable machining processes can help machining companies to obtain financial and environmental benefits, because the sustainable machining techniques have the features of eco-friendly, waste-free, nonlethal, cost-effective, and energy-

efficient [1]. The metal cutting processes are energy-intensive. The mismatch between the constant increase of energy consumption and the shortage of new energy sources in the world had become more and more incisive in recent years [2]. Furthermore, Balogun et al. stated that the production and consumption of energy intensified environmental pollution [3]. Therefore, reducing energy consumption is of crucial importance in the metal cutting process for implementing sustainable machining.

Over the last decades, researchers have put forward several methods to improve sustainability in metal cutting processes. Minimum quantity lubrication (MQL)-assisted machining has been recommended by different researchers [4]. The high-velocity fluid droplets can penetrate the vapor blanket, and reach into tool-work interfaces, which can provide a better tribology and heat transfer than wet lubrication. The compressed air can remove metal chips from the machining zone [5]. Cryogenic cutting was another new sustainable machining theory. Mia et al. studied the cutting force, specific energy, temperature, surface quality (i.e., surface roughness), and material removal rate of Ti-6Al-4V under the impingement of

✉ Shufeng Sun  
shufeng2001@163.com

<sup>1</sup> School of Mechanical & Automotive Engineering, Key Lab of Industrial Fluid Energy Conservation and Pollution Control (Ministry of Education), Qingdao University of Technology, Qingdao 266033, China

<sup>2</sup> Manufacturing and Automation Research Laboratory, Department of Industrial and Systems Engineering, Rutgers University, Piscataway, NJ 08854, USA

<sup>3</sup> School of Mechanical Engineering, University of Jinan, Jinan 250022, China

cryogenic liquid nitrogen (LN2) and found that LN2 dual jets were effective in reducing the specific energy consumption and temperature and improving surface quality [6]. Minimum quantity cooling lubrication (MQCL) technique combined the benefits of MQL and cryogenic cutting methods to achieve good tribology and cooling effects [7].

In recent years, micro-texturing on cutting tool surfaces has been another efficient technique to achieve sustainable machining in metal cutting field. Hao et al. suggested that the micro-textures can enhance the tribological conditions between the cutting tool surfaces and the workpiece or chip surfaces [8]. Xing et al. all concluded that the micro-textures on tool rake face can reduce the friction of coefficient between workpiece and cutting tools, thus reducing the cutting forces [9–11]. The specific cutting energy, which indicates the energy consumption of removing the workpiece material per unit volume, is a common measure of energy efficiency in machining processes [12, 13]. Lower specific cutting energy indicates a higher energy efficiency and better sustainability of the machining process. It is known that the experimental specific cutting energy  $E_u$  can be calculated based on the cutting forces by (1).

$$E_u = \frac{F_c}{a_p a_w} \quad (1)$$

where  $F_c$  is the cutting force in cutting velocity direction and  $a_p$  and  $a_w$  are the depth of cut and cutting width, respectively. Therefore, the micro-textured cutting tools can reduce the specific cutting energy consumption by reducing the cutting forces, thus implementing green manufacturing in cutting processes.

Although various micro-texture designs have been investigated in cutting processes to obtain a low cutting force, a common shortage was found by researchers. Since the cutting tool surfaces were usually a plane, the micro-textures will generate sharp edges/corners between the cutting tool surfaces and the texture sidewalls. Once the chips were plugged into the micro-texture valleys, these sharp edges/corners would cut into the chips and generate derivative cutting processes [14, 15]. The derivative cutting processes could impede the flow of chips and produce extra cutting forces, weakening the benefits of micro-textures on sustainable machining. Sasi et al. also confirmed this phenomenon by checking the deformed back surfaces of chips and the filled micro-textures after cutting with textured tools [16, 17].

Given the derivative cutting processes generated by micro-textures, Liu et al. have designed a new kind of curvilinear micro-grooves on cutting tool rake face to eliminate derivative cutting processes and implement sustainable turning processes by three-dimensional (3D) finite element (FE) simulation [18]. The simulation results proved that, both under rough and finish turning conditions, the new curvilinear micro-grooved cutting tools could reduce the cutting forces more

significantly than traditional linear micro-grooved tools during turning stainless steel 17-4PH. The curvilinear micro-grooved cutting tool was a more appropriate choice for achieving green manufacturing than non-textured and linear micro-grooved tools. However, there are mainly two deficiencies remaining in their work. Firstly, the curvilinear micro-grooved cutting tools were not physically fabricated, and their cutting performance was not tested experimentally. Secondly, the simulation results showed that the cutting performance of curvilinear micro-grooved tools with same parameters was different in rough and finish turning processes which needed further clarification. Therefore, micro-groove parameters should be optimized according to the cutting conditions for roughing and finish turning separately.

To counter the deficiencies above, this paper studied the preparation method of curvilinear micro-grooves on cemented carbide tool rake faces. Meanwhile, the specific cutting energy was adopted as the target to optimize the curvilinear micro-groove parameters in rough and finish turning conditions by 3D FE simulations. At last, the preparation method was adopted to fabricate the optimal curvilinear micro-grooved cutting tools, and their cutting performance was investigated experimentally in turning stainless steel 17-4PH. This work is a follow-up work of our previous work [18] and the research methodology is shown in Fig. 1.

## 2 Fabrication method for curvilinear micro-groove textures

Several machining methods have been adopted in the existing literature to fabricate micro-/nano textures on cutting tool rake faces. Kümme et al. adopted the laser micro-machining method [19–21], and Li et al. used micro-EDM machining technology [22, 23]. The micro-grinding and focused ion beam machining were adopted by Xie et al. [16] and Kawasegi et al. [24], respectively. Among these machining technologies, the femtosecond laser was more suitable to fabricate micro-textures on uncoated carbide tools due to its advantages, e.g., limited heat-affected zone and high machining precision. Therefore, a femtosecond laser system (Spectra-Physics, Newport Corporation, USA) was used in this work to fabricate curvilinear micro-grooves on cutting tool rake faces. This system has a wavelength of 800 nm, pulse duration of 35 fs, single pulse energy of up to 13 mJ, and maximum repetition rate of 1 kHz. A lens of  $\times 40$  and numerical aperture (NA) of 0.75 was adopted to focus the beam on insert surfaces with the radius of focus spot of 1.5  $\mu\text{m}$ . A 3D XYZ stage with a precision of 80 nm was used to move the cutting tool. The machining was conducted in air environment under atmospheric pressure.

Compared with the traditional linear micro-grooves, the arc surfaces (see Fig. 2) on the curvilinear micro-grooves were the

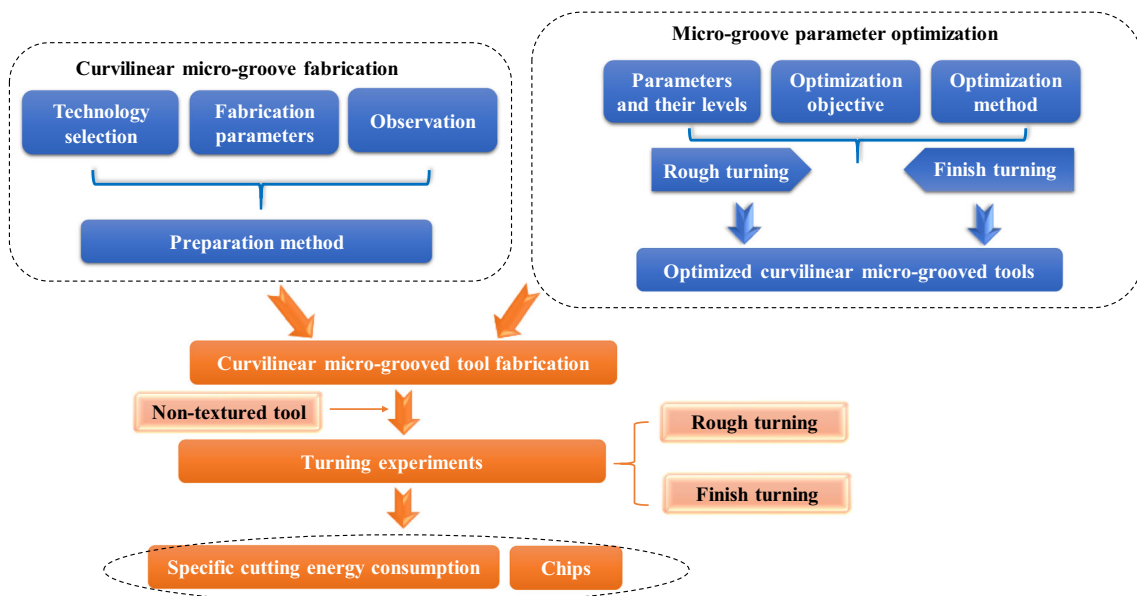


Fig. 1 Research methodology of this work

difficulties of machining. In this work, a two-step method was developed to fabricate the curvilinear micro-grooves. Firstly, the linear micro-grooves were shaped with layer-by-layer scan machining. In each layer, the laser scanned in the direction of micro-groove length and fed along the width direction. The feed rate was determined by pilot experiments to match with the kerf width. After finishing a layer, the laser fed in the depth direction and repeated the above scan machining. The feed rate in depth direction and the layer number were also determined by pilot experiments. Figure 3 shows the principle diagram of layer-by-layer scan machining for linear micro-grooves.

After obtaining the linear micro-grooves, the arc surfaces were produced based on the asymptotic fitting method. The cross-sectional geometries of machining marks, induced by femtosecond laser with different scanning parameters, were firstly measured by a KEYENCE VK-X200 K laser microscope and then fitted by Gaussian equations, since the pulse energy of femtosecond laser nearly satisfied the Gaussian distribution. After that, the MATLAB software was used to fit the circular arcs by the fitted Gaussian equations to determine the femtosecond laser machining parameters of the arc

surfaces on curvilinear micro-grooves. The principle diagram of the asymptotic fitting method is shown in Fig. 4.

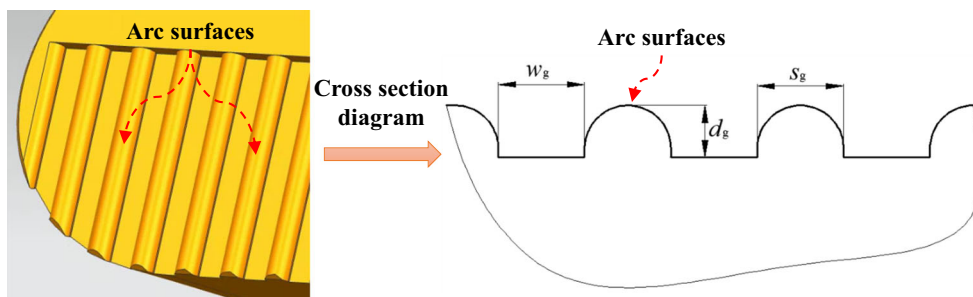
Figure 5 shows the 3D geometry of the produced curvilinear micro-grooved inserts used in our preliminary work, in which design parameters were micro-groove width  $w_g = 50 \mu\text{m}$ , spacing  $s_g = 50 \mu\text{m}$ , depth  $d_g = 50 \mu\text{m}$ , and edge distance  $t_g = 0$ . As shown in Fig. 6, the machined geometry of the curvilinear micro-grooves was highly consistent with the original design, indicating that the curvilinear micro-groove preparation method developed above is very effective.

### 3 Methodology for micro-groove geometry optimization

#### 3.1 Micro-groove parameter optimization

Finite element (FE) modeling has been widely utilized to analyze the influence of micro-textured tools on the cutting process and to evaluate the effect of micro-textures on cutting force, temperature, friction coefficient, and chip morphology.

Fig. 2 Geometry of the designed curvilinear micro-grooves



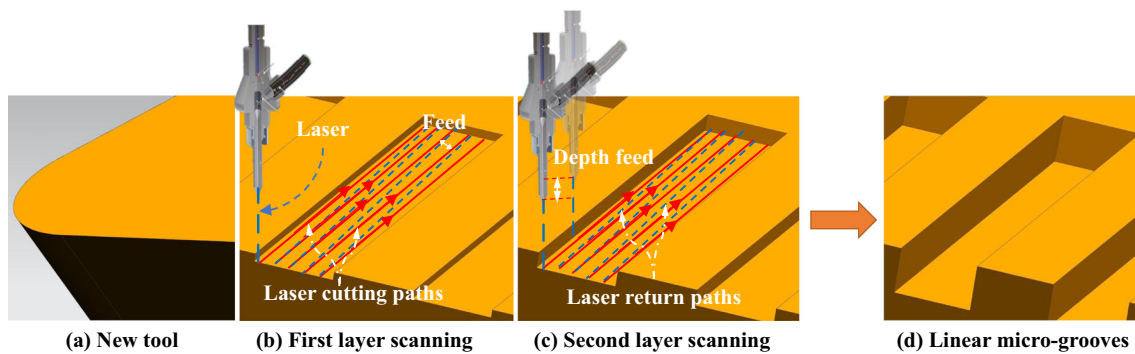


Fig. 3 Principle diagram of layer-by-layer scan machining for linear micro-grooves

Patel et al. [25] and Arulkirubakaran et al. [26] both used DEFORM-3D software to simulate the performance of micro-textures in machining of titanium alloy Ti6Al4V. Liu et al. analyzed the performance of newly designed cutting tools with a curvilinear micro-grooved surface with 3D FE simulations in AdvantEdge software [18]. These attempts show that FE modeling and simulations have a great potential for providing good assistance in designing cutting tools with new texture patterns and assessing their performance virtually.

The optimization of curvilinear micro-groove parameters was conducted by 3D FE simulations with a nose turning module in AdvantEdge FEM software (see Fig. 6). Based on the previous work [18], the self-defined J-C material model of stainless steel 17-4PH (see Eq. (2)) and the mechanical properties in Table 1 were implemented into the FEM model of cutting to define the workpiece material. The friction coefficient was fixed at 0.4.

$$\sigma = (1279 + 630\varepsilon^{0.64}) \left[ 1 + 0.02 \ln \left( \frac{\dot{\varepsilon}}{0.001} \right) \right] \left[ 1 - \left( \frac{T-20}{1400} \right)^{0.56} \right] \quad (2)$$

where  $\sigma$  is the flow stress,  $\varepsilon$  is the plastic strain,  $\dot{\varepsilon}$  is the plastic strain rate, and  $T$  is the temperature.

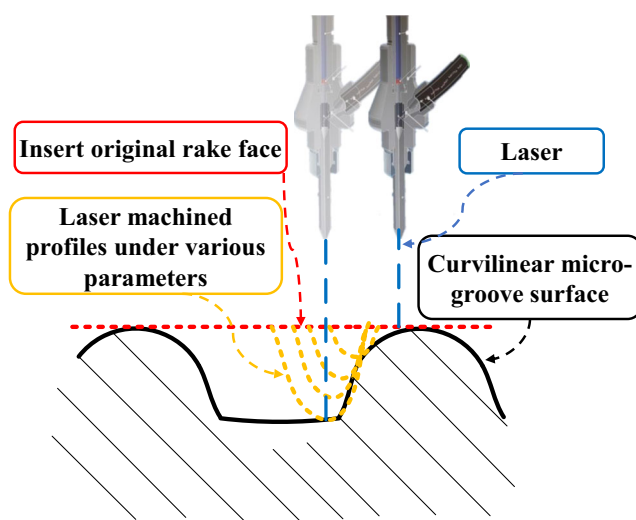


Fig. 4 Principle diagram of asymptotic fitting method for machining arc surfaces of curvilinear micro-grooves

The curvilinear micro-groove parameters were optimized under two different sets of cutting parameters respectively: (i) the rough turning at a cutting speed ( $v$ ) of 80 m/min, a feed rate ( $f$ ) of 0.2 mm/rev, and a depth of cut ( $a_p$ ) of 1 mm and (ii) the finish turning at  $v = 150$  m/min,  $f = 0.1$  mm/rev and  $a_p = 0.4$  mm.

According to the inserts (Kennametal TPGN110304 K313 uncoated carbide inserts) and tool holder (CTGPR2020K11) that were planned to be used in subsequent cutting experiments, the basic geometry in Table 2 and the standard Grade K cemented carbide were used to define the cutting tool. According to our preliminary work, the micro-grooves in the direction of perpendicular to main cutting edge could improve the cutting performance more significantly than parallel micro-grooves, and the bottom shape of the micro-grooves had no obvious effects on the cutting performance [23]. Therefore, the perpendicular micro-grooves with curvilinear surface and linear bottom cross-sections were adopted as the basis in this work. The optimization micro-groove parameters include the micro-groove width ( $w_g$ ), spacing ( $s_g$ ), depth ( $d_g$ ), and edge distance ( $t_g$ ). The single factor design with four levels of each micro-groove parameter, as shown in Table 3, was employed in both rough and finish turning conditions.

During all the simulations, adaptive meshing technique was used in the cutting zone to obtain fine meshes, with the minimum and maximum element size of 0.0005 mm and 0.01 mm, respectively. The simulative length of cut for each cutting process was maintained as 2 mm, and no cooling and lubricating action was applied.

### 3.2 Cutting experiment design for verification

Since the laser processing can destroy the tool coating and thus influence the experimental result, the optimized curvilinear micro-grooves were fabricated on the rake faces of Kennametal TPGN110304 K313 uncoated carbide inserts by the method developed in Section 2. The original and curvilinear micro-grooved inserts were mounted on a tool holder of CTGPR2020K11 to turn the solution and aging treated stainless steel 17-4PH bar with a diameter of 50 mm. The rough and finish turning parameters used in the above FE

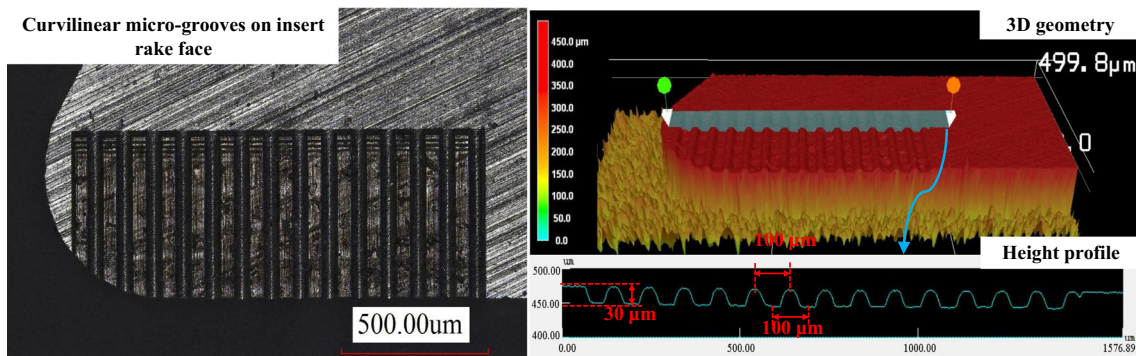


Fig. 5 Geometry of prepared curvilinear micro-grooved inserts with the design parameters of  $w_g = 50 \mu\text{m}$ ,  $s_g = 50 \mu\text{m}$  and  $d_g = 50 \mu\text{m}$

simulations were adopted in the cutting experiments. All the cutting experiments in this work were conducted on a CAK3536 rigid CNC turning center with the cylindrical turning mode. Its schematic diagram is shown in Fig. 7. No cutting fluid was used in all cutting processes.

The cutting force in cutting velocity direction,  $F_c$ , for each cutting condition was measured with a YDC-III89B three-component piezoelectric dynamometer for three times. The sampling frequency of the dynamometer was set as 1000 Hz. The average value and standard deviation of the specific cutting energy were calculated using the  $F_c$  based on Eq. (1). The chip back surfaces (the surfaces in contact with the cutting tool rake faces) were observed using a KEYENCE VK-X200 K laser microscope to check the deformation degree and evaluate the effects of micro-grooves. After finishing the cutting processes, the inserts were observed by the laser microscope to ensure there was no severe tool wear.

## 4 Results and discussion

### 4.1 Effect of curvilinear micro-groove width on the specific cutting energy

Figure 8 shows the effects of curvilinear micro-groove width on the average specific cutting energy in rough and finish turning of stainless steel 17-4PH, and the error bar shows

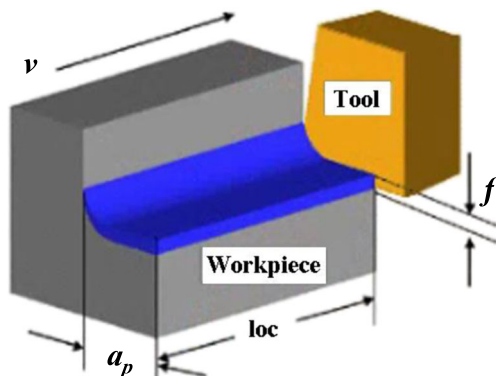


Fig. 6 Schematic diagram of the 3D FE model

the standard deviation of each point. It can be seen that the trends of specific cutting energy against the micro-groove width were different in these two conditions. In finish turning, the specific cutting energy increased overall with the enlarged micro-groove width within the studied range. It indicated that the curvilinear micro-groove with a minimum width of  $20 \mu\text{m}$  was suitable for achieving the highest sustainability in terms of lower specific cutting energy. While in rough turning, the specific cutting energy decreased firstly and then increased with the micro-groove width increasing from  $20 \mu\text{m}$  to  $110 \mu\text{m}$ . The lowest specific cutting energy consumption was achieved at the micro-groove width of  $50 \mu\text{m}$ , which could be selected to implement green rough turning of stainless steel 17-4PH.

It has been found that the micro-grooves on cutting tool rake faces reduced the specific cutting energy mainly via reducing the tool-chip contact area, while the interaction between the deformed chips and micro-groove side/bottom walls could weaken these beneficial effects [18]. Therefore, the distributions of contact stresses on cutting tool rake faces can be employed to show the contact conditions on tool-chip interfaces and further reveal the influence mechanism of curvilinear micro-groove parameters on the specific cutting energy. Figure 9 and Fig. 10 show the rake face stress distributions of curvilinear micro-grooved cutting tools with various widths in rough and finish turning conditions, respectively. The purple arrows show the chip flow direction, and  $\theta_i$  is the angle of inclination relative to the micro-grooves. The white solid arrows in Fig. 9 show the average tool-chip contact length, which was obtained based on the rake face stress distributions. The spotty distribution of high stress regions should be attributed to the tool-chip contact discontinuities, which was due to the grooved tool rake face geometry. This result agreed well with Haddag et al., who have found this phenomenon when turning with grooved inserts [27, 28]. It can be seen that during rough turning, the nose radius edge showed some effects on the chip flow direction and resulted in an angle of inclination between the chip flow direction and the micro-grooves. It must be noted that the values of the angles were slightly different with various micro-groove structures because of the

**Table 1** The mechanical properties of the stainless steel 17-4PH

Property	Value	Property	Value
Density (kg/m <sup>3</sup> )	7780	Young modulus (GPa)	191
Yield strength (MPa)	1235	Poisson's ratio	0.272
Tensile strength (MPa)	1425	Linear expansion coefficient (°C <sup>-1</sup> )	1.136 × 10 <sup>-5</sup>
Hardness (HRC)	43	Elongation (%)	12

different tool-chip friction conditions. Under finishing turning conditions, the chips started to flow along the micro-grooves when the micro-groove width reached 50 μm, since the chips were plugged into the micro-groove valleys (which will be discussed below).

It can be seen from Fig. 9a–b that when the micro-groove width was 20 μm and 50 μm, the high stress areas mainly appeared on the arc-shipped upper surfaces of the micro-grooves and there was almost no high stress region at micro-groove bottoms. This indicated that the chips mainly flowed on the cutting tool rake faces without severely deforming into the micro-groove valleys and interacting with the bottom surfaces. In this case, the large micro-groove width reduced the tool-chip contact area and thus reduced the specific cutting energy, see Fig. 8. When the micro-groove width further increased to 80 μm or 110 μm, the oversized micro-groove valleys led the chips to be plugged into the valleys and interact with the micro-groove side/bottom walls (see the high stress regions at micro-groove bottoms in Fig. 9c–d). The interaction between the deformed chips and micro-groove side/bottom surfaces increased the tool-chip friction, resulting in the higher consumption of specific cutting energy. The tool-chip contact length observation results confirmed above conclusions. It can be seen from Fig. 9 that when the micro-groove width increased from 20 to 50 μm, the tool-chip contact length decreased lightly. But when the micro-groove width further increased to 80 μm and 110 μm, the tool-chip contact length increased significantly and the chips even reached the top edge of the micro-grooved region. According to Xing et al. [29], there is a moment  $M$ , induced by the non-colinear resultant forces acting at tool rake face and shear plane, that made the chip curl. The reduced tool-chip friction will increase the moment  $M$  and thus make the chip curling increased, which will shorten the tool-chip contact length. In other words, the longer tool-chip contact length indicated the larger friction.

**Table 2** The cutting tool geometry parameters

Insert nose radius (mm)	Relief angle (°)	Side rake angle (°)	Back rake angle (°)	Lead angle (°)
0.4	6	5	5	0

**Table 3** The single factor design for optimizing curvilinear micro-groove parameters

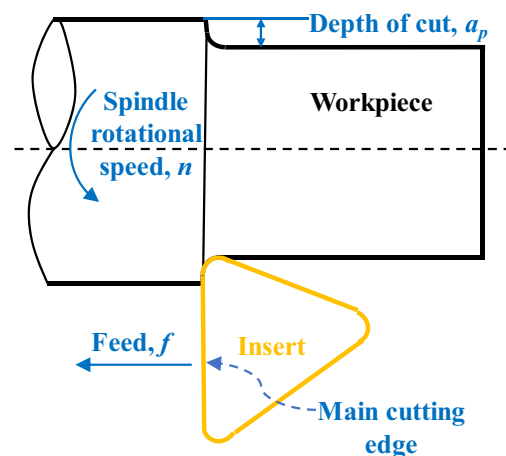
	Group I	Group II	Group III	Group IV
$w_g$ (μm)	20, 50, 80, 110	50	50	50
$s_g$ (μm)	50	20, 50, 80, 110	50	50
$d_g$ (μm)	30	30	10, 30, 50, 70	30
$t_g$ (μm)	0	0	0	0, 50, 100, 150

Therefore, the tool-chip contact length observation results in Fig. 9 suggested that the tool-chip friction forces slightly decreased first and then increased dramatically when the micro-groove width increased from 20 to 110 μm, agreeing well with the consumption of specific cutting energy in Fig. 8.

In the case of finish turning, it can be seen from Fig. 10 that the high stress regions at the micro-groove bottoms appeared initially when the micro-groove width was 50 μm. This indicated that the chips started to be plugged into the micro-groove valleys at the micro-groove width of 50 μm because of the low rigidity of the thin chips. In this case, the larger micro-groove width could result in the more severely deformed chips and enhance their interaction with the micro-groove side/bottom surfaces, giving rise to the increased specific cutting energy continuously (see Fig. 8).

#### 4.2 Effect of curvilinear micro-groove spacing on the specific cutting energy

Figure 11 displays the effects of curvilinear micro-groove spacing on the specific cutting energy in rough and finish turning of stainless steel 17-4PH. Unlike the effects of micro-groove width, the variation trends of specific cutting energy along with the micro-groove spacing in rough and finish turning conditions were the same. The specific cutting energy continuously increased with increasing micro-groove spacing within the tested range. Therefore, the spacing of

**Fig. 7** Schematic diagram of the cylindrical turning

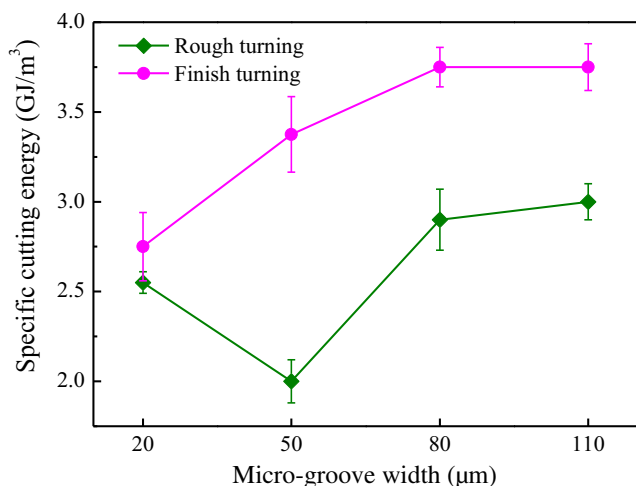


**Fig. 8** Effects of curvilinear micro-groove width on the specific cutting energy in rough and finish turning of stainless steel 17-4PH

20 μm was the best choice for curvilinear micro-grooved cutting tools to achieve green manufacturing in both rough and finish turning processes.

The rake face stress distributions of curvilinear micro-grooved cutting tools with various spacings under rough and finish turning conditions are shown in Fig. 12 and Fig. 13, respectively. The purple arrows show the chip flow direction, and  $\theta_i$  is the angle of inclination relative to the micro-grooves. The white solid arrows in Fig. 12 show the average tool-chip contact length. Similar to the effect of micro-groove width, there was an angle of inclination between the chip flow direction and the micro-grooves during rough turning, with different values. Under finishing turning conditions, the chips started flow along the micro-grooves when the micro-groove spacing reached 50 μm.

It can be seen that the obvious high stress regions at micro-groove bottoms appeared initially at a micro-groove spacing of 80 μm for rough turning and 50 μm for finishing turning. Above this critical value, the enlarged micro-groove spacing could lead to more serious interaction between chips and micro-groove side/bottom walls. This can weaken the beneficial effects of micro-grooves on friction reduction and increase the specific cutting energy consumption. Therefore,

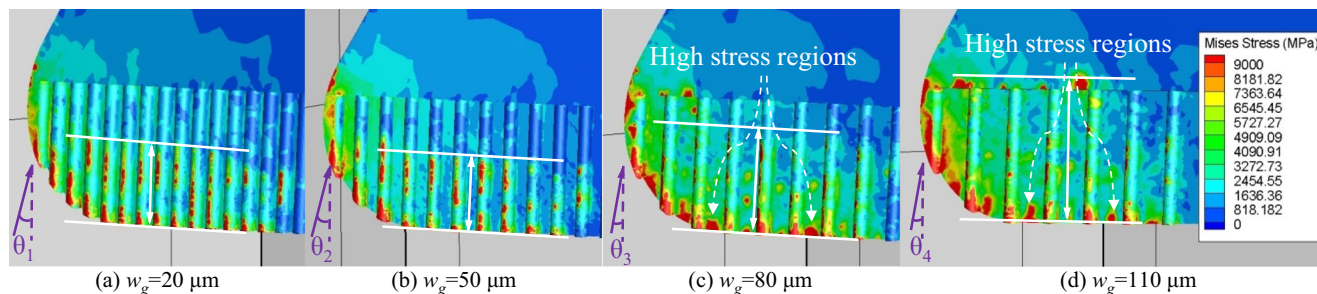
the specific cutting energy increased with the micro-groove spacing increasing from 50 to 110 μm under rough turning conditions and from 20 to 110 μm under finish turning conditions, as shown in Fig. 11.

These results were confirmed by the average tool-chip contact length in Fig. 12. The inner link of tool-chip friction and tool-chip contact length has been discussed in Section 4.1. Therefore, the enlarged tool-chip contact length indicated that the total friction force in tool-chip interface increased significantly when the micro-groove spacing increased from 50 to 110 μm in rough turning conditions. As a result, the specific cutting energy increased as well.

When the micro-groove spacing increased from 20 to 50 μm in rough turning conditions, the large micro-groove spacing increased the radius of the arc-shaped upper surfaces, which could increase the contact area between chips and micro-texture upper surfaces with the same deformation degree of chips. In addition, although the chips did not interact with the micro-groove bottoms, the large micro-groove spacing could increase the chip deformation degree and increase the tool-chip contact area. The combination of these two factors resulted in the higher specific cutting energy when the micro-groove spacing increased from 20 to 50 μm in rough turning conditions.

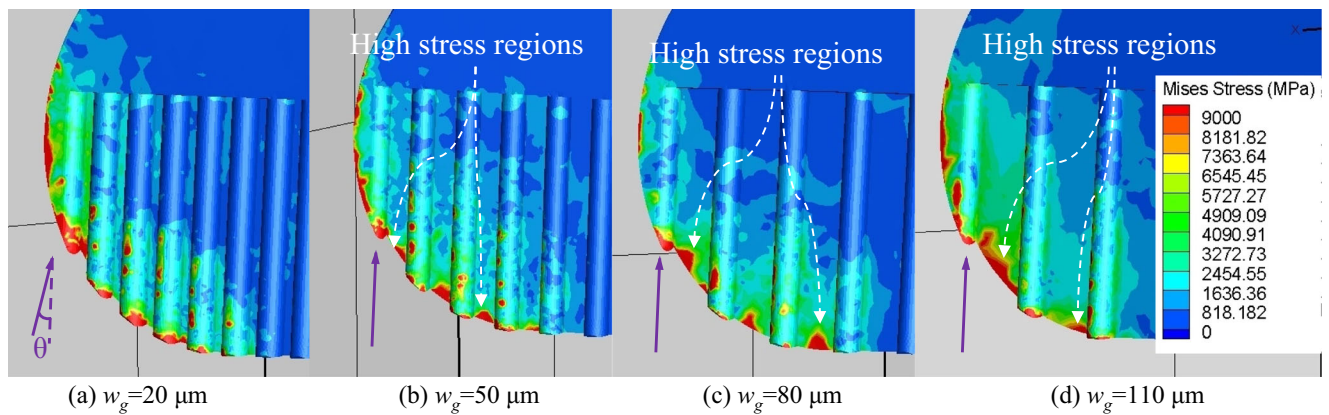
### 4.3 Effect of curvilinear micro-groove depth on the specific cutting energy

Figure 14 shows the curvilinear micro-groove depth dependence of the specific cutting energy in rough and finish turning of stainless steel 17-4PH. It is obvious that the effects of micro-groove depth on the specific cutting energy consumption under rough and finish turning conditions were the same, i.e., the specific cutting energy firstly decreased when the micro-groove depth increased from 10 to 30 μm and then remained stable in general against the further deepened micro-grooves. In order to achieve the highest sustainability in turning stainless steel 17-4PH, the micro-groove depth of 30 μm was selected as the optimized curvilinear micro-groove depth for both rough and finish turning conditions.



**Fig. 9** Effect of micro-groove width on tool stress distributions in rough turning (The purple arrows show the chip flow direction, and  $\theta_i$  is the

angle of inclination relative to the micro-grooves. The white solid arrows show the tool-chip contact length.)



**Fig. 10** Effect of micro-groove width on tool stress distributions in finish turning (The purple arrows show the chip flow direction, and  $\theta$  is the angle of inclination relative to the micro-grooves.)

The micro-groove depth can influence the specific cutting energy consumption mainly via the interaction between the deformed chips and the micro-groove side/bottom surfaces. With the fixed cutting condition and micro-groove width and spacing, there will be a maximum depth of chip deformation if the chip deformation is not limited by the micro-groove bottom.

If the micro-groove depth is lower than the above-assumed maximum depth, the deformed chips will reach the micro-groove bottom and interact with the micro-groove side and bottom faces. In this case, the deeper micro-grooves will weaken the interaction between the chips and micro-groove bottoms but increase the contact area between the chips and micro-groove side walls. There should be a critical micro-groove depth that balances the abovementioned opposite effects and achieves the minimal specific cutting energy consumption. When the micro-groove is deeper than this critical micro-groove depth, the abovementioned opposite effects offset each other and maintain the minimal specific cutting energy consumption.

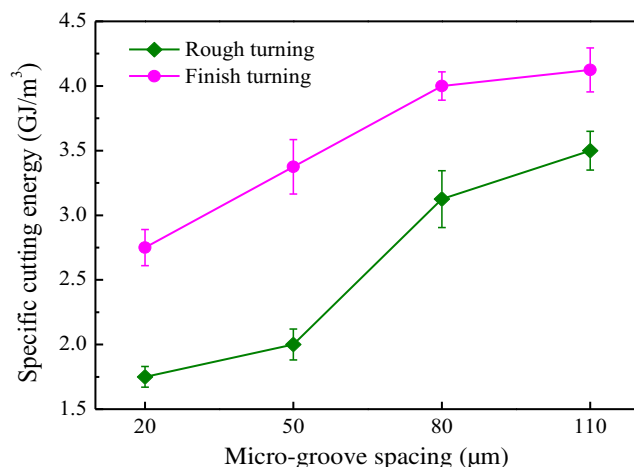


**Fig. 11** Effects of curvilinear micro-groove spacing on the specific cutting energy in rough and finish turning of stainless steel 17-4PH

If the micro-groove depth is larger than the above-assumed maximum depth, the deformed chips will not reach the micro-groove bottom. In this case, the changed micro-groove depth will not affect the chip deformation and thus show no effect on the specific cutting energy.

From the above, under both rough and finish turning conditions, the specific cutting energy decreased firstly and then generally remained stable with an increase of micro-groove depth, as shown in Fig. 14.

#### 4.4 Effect of curvilinear micro-groove edge distance on the specific cutting energy

Figure 15 shows the effects of curvilinear micro-groove edge distance on the specific cutting energy in rough and finish turning of stainless steel 17-4PH. With increasing edge distance, the specific cutting energy consumption significantly increased firstly (see Fig. 15 for edge distance increasing from 0 to 50 μm) and then slightly increased under both rough and finish turning conditions. When only the specific cutting energy is considered, the curvilinear micro-grooves with an edge distance of 0 should be undoubtedly selected.

It is well-known that the stress distributions along the tool-chip contact area can be represented as Fig. 16: the normal stress,  $\sigma_n$ , declined continuously along with the increased distance to the cutting edge, while the shear stress,  $\tau_f$ , remained stable with a high value at first (sticking region) and then declined with an increase of edge distance (sliding region) [30]. The maximal tool-chip interaction located near the cutting edge and gradually weakened with the increased edge distance. Therefore, when the micro-groove edge distance increased from 0 to 50 μm, the positive effects of curvilinear micro-grooves on reducing tool-chip friction were notably weakened, resulting in the significantly enlarged specific cutting energy. After that, the further increased micro-groove edge distance reduced the beneficial effects gradually and led to the slightly increased specific cutting energy.



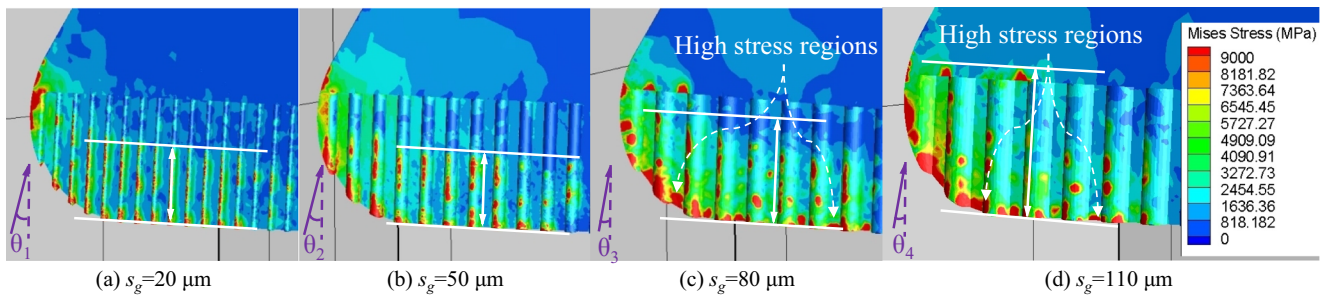


**Fig. 12** Effect of micro-groove spacing on tool stress distributions in rough turning (The purple arrows show the chip flow direction, and  $\theta_i$  is the angle of inclination relative to the micro-grooves. The white solid arrows show the tool-chip contact length.)

### 4.5 Curvilinear micro-groove optimization and experimental verification

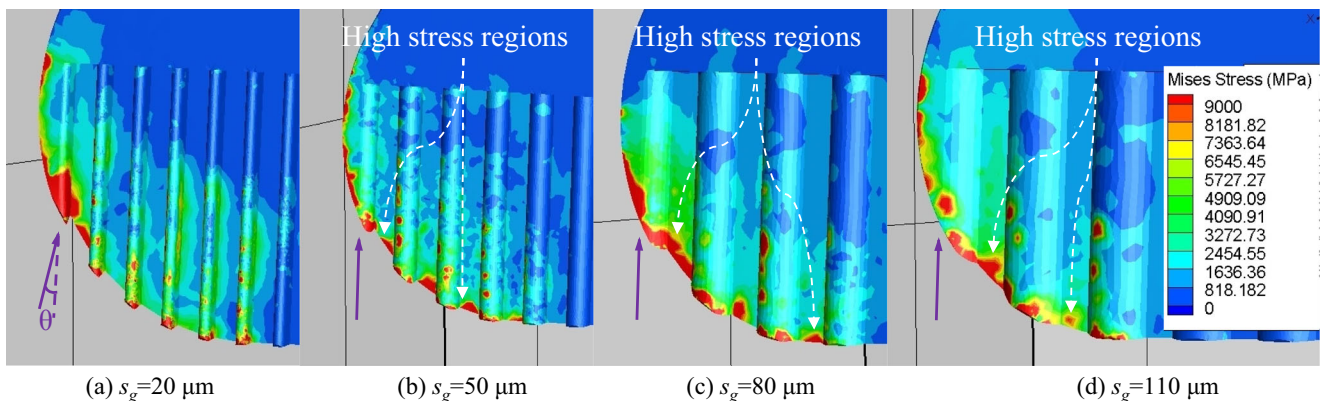
Based on the simulative specific cutting energy analysis under different micro-groove width, spacing, depth, and edge distance (see Figs. 8, 11, 14 and 15, respectively), the optimal curvilinear micro-groove parameter combinations for achieving highest energy efficiency in turning stainless steel 17-4PH were determined and shown in Table 4.

Figure 17 exhibits the experimental and simulative specific cutting energy by the optimized curvilinear micro-grooved inserts and non-textured inserts in rough and finish turning conditions. It can be seen that good agreements between the experimental and simulative results were obtained in both rough and finish turning processes. In addition, the experimental and simulative results both indicated that the optimal curvilinear micro-grooved cutting tools could obviously reduce the specific cutting energy in both rough and finish turnings, confirming the accuracy of the optimal results.

It has been put forward above that the curvilinear micro-groove parameters influenced the specific cutting energy mainly by the interaction between the deformed chips and micro-groove side/bottom surfaces. The optimal curvilinear

micro-grooves can achieve the lowest specific cutting energy consumption by restraining the chip deformation and thus reduce the tool-chip contact area. Therefore, the back surface geometries of chips obtained from rough and finish turning processes using the optimal curvilinear micro-grooved inserts were observed and shown in Fig. 18.

It can be seen from Fig. 18a that some patterned micro-grooves formed on chip back surfaces in rough turning conditions. This structure was derived from the micro-grooves on tool rake faces and indicated that the chips were plugged into the micro-groove valleys. This should be one of the reasons why the experimental specific cutting energy was higher than that of simulative results with micro-grooved inserts (see Fig. 17a). However, the height profile measurement in Fig. 18a showed that the heights of the patterned micro-grooves on chip back surfaces were no more than 10  $\mu\text{m}$ , much less than the curvilinear micro-groove depth ( $d_g = 30 \mu\text{m}$ ). Therefore, the deformation degree of the chips was restrained and the interaction between chips and micro-groove bottoms were eliminated, agreeing with the optimal results. In addition, the surfaces of the patterned micro-grooves on chip back faces were smooth and no burr was found, proving that no derivative cutting process was induced by the micro-textures. This



**Fig. 13** Effect of micro-groove spacing on tool stress distributions in finish turning (The purple arrows show the chip flow direction, and  $\theta$  is the angle of inclination relative to the micro-grooves.)

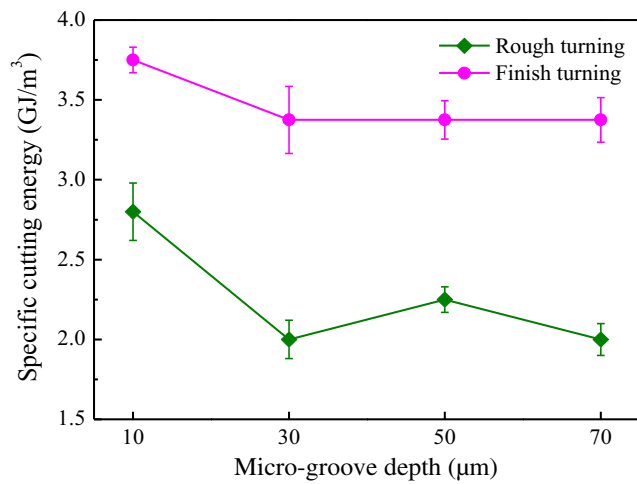


**Fig. 14** Effects of curvilinear micro-groove depth on the specific cutting energy in rough and finish turning of stainless steel 17-4PH

result agreed with the initial design concept of curvilinear micro-grooves, i.e., eliminating derivative cutting processes by arc-shaped upper surfaces.

In the finish turning condition, the results in Fig. 18b showed that no obviously patterned structure was formed on chip back faces, indicating that the deformation of chips into micro-groove valleys was basically eliminated by the small micro-groove width and spacing. The result analysis of Fig. 18 indicated that the curvilinear micro-groove optimization mechanism was accurate.

### 5 Conclusions

In this paper, the curvilinear micro-grooves used on cutting tool rake faces were optimized and fabricated for implementing sustainable machining, as a follow-up work of

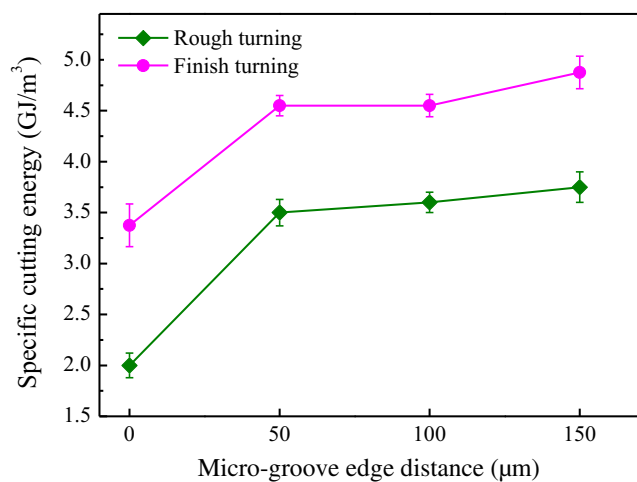


**Fig. 15** Effects of curvilinear micro-groove edge distance on the specific cutting energy in rough and finish turning of stainless steel 17-4PH

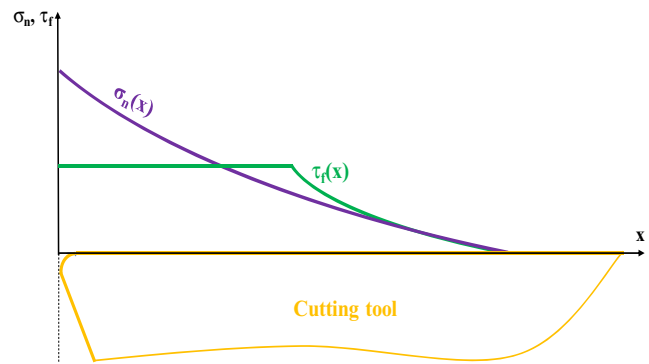


**Fig. 16** Normal ( $\sigma_n$ ) and shear ( $\tau_f$ ) stress distributions on tool rake face [27]

our previous work [18]. The effect rules and mechanism of curvilinear micro-groove width, spacing, depth, and edge distance on specific cutting energy during turning stainless steel 17-4PH were investigated. The main findings of this work are summarized as follows:

- (1) A two-step preparation methodology was creatively developed to fabricate the curvilinear micro-grooves on carbide tool rake faces with a femtosecond laser, which combined the layer-by-layer scan machining and asymptotic fitting principle. The highly consistent geometry between the prepared curvilinear micro-grooves and their original designs proved that the new preparation method was effective. However, it must be noted that the processing efficiency of curvilinear micro-grooves fabrication with femtosecond laser was relatively low and the further research about high effective machining technology is needed.
- (2) The influence of curvilinear micro-groove parameters, including the micro-groove width, spacing, depth, and edge distance, on the specific cutting energy during turning stainless steel 17-4PH were revealed under rough and finish turning conditions, respectively. It was found that the effect rules were not fully consistent under rough and finish turning conditions. In rough turning, the specific cutting energy decreased at first and then increased with the increased micro-groove width. The lowest specific cutting energy consumption was obtained at the micro-groove width of 50 μm. While in finish turning condition, the larger the micro-groove width, the higher specific cutting energy was obtained. When the micro-

**Table 4** The optimal curvilinear micro-groove parameter combinations

	$w_g$ (μm)	$s_g$ (μm)	$d_g$ (μm)	$t_g$ (μm)
Rough turning	50	20	30	0
Finish turning	20	20	20	0

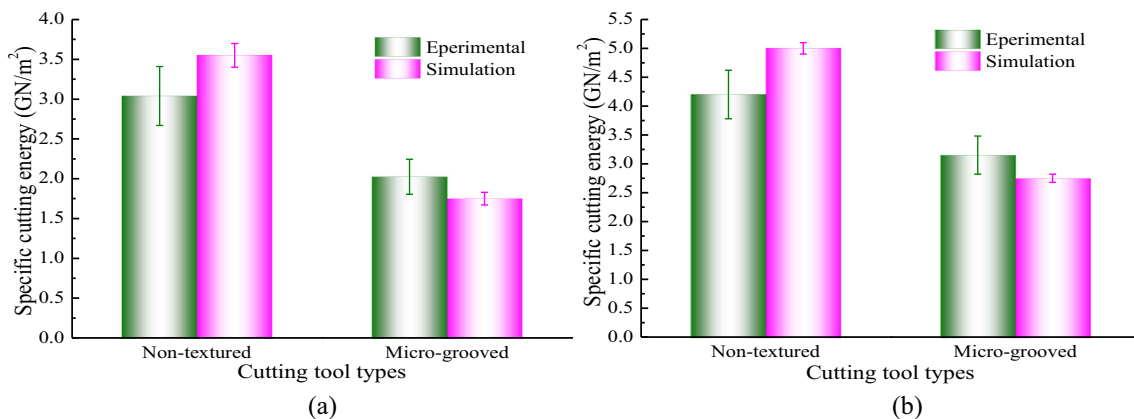


Fig. 17 Experimental and simulative specific cutting energy with optimal curvilinear micro-grooved inserts in **a** rough and **b** finish turning of stainless steel 17-4PH.

groove spacing or edge distance was enlarged, the specific cutting energy continuously increased in both rough and finish turning conditions. The specific cutting energy declined firstly and then remained stable in general against the deepened micro-grooves under both rough and finish turning conditions. The lowest value was obtained at the micro-groove depth of 30 μm.

- (3) The effect mechanism of curvilinear micro-groove parameters on specific cutting energy was revealed and

the optimal curvilinear micro-groove structures were recommended under rough and finish turning conditions, respectively. It was found that the optimal curvilinear micro-grooves reduced the specific cutting energy by restraining the tool-chip contact area and eliminating the derivative cutting processes. The optimal curvilinear micro-groove structures for implementing green manufacturing in dry turning of stainless steel 17-4PH were  $w_g = 50 \mu\text{m}$ ,  $s_g = 20 \mu\text{m}$ ,  $d_g = 30 \mu\text{m}$ , and  $t_g = 0$  for

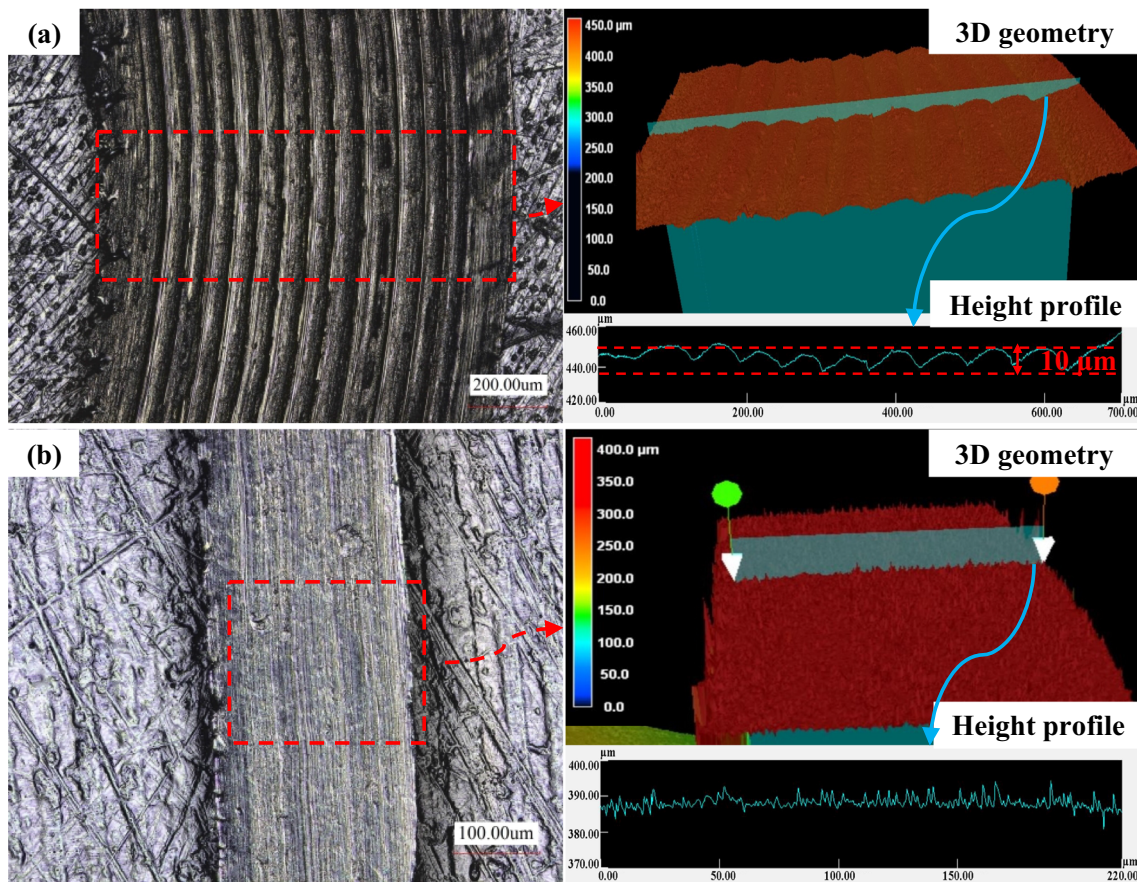


Fig. 18 Back surface geometry of chips obtained from **a** rough and **b** finish turning processes with optimal curvilinear micro-grooved inserts

rough turning condition and  $w_g = 20 \mu\text{m}$ ,  $s_g = 20 \mu\text{m}$ ,  $d_g = 30 \mu\text{m}$ , and  $t_g = 0$  for finish turning condition.

**Acknowledgment** We appreciate the support of Key Lab of Industrial Fluid Energy Conservation and Pollution Control at Qingdao University of Technology (Ministry of Education).

**Funding information** This work is financially supported by the National Natural Science Foundation of China (51775289 and 51705272), Taishan Scholars Program (TS201511038), and Postdoctoral Applied Research Project of Qingdao.

## References

- Chetan GS, Venkateswara RP (2015) Application of sustainable techniques in metal cutting for enhanced machinability: a review. *J Clean Prod* 100:17–34
- Wang B, Liu Z, Song Q, Wan Y, Shi Z (2016) Proper selection of cutting parameters and cutting tool angle to lower the specific cutting energy during high speed machining of 7050-T7451 aluminum alloy. *J Clean Prod* 129:292–304
- Balogun VA, Mativenga PT (2013) Modelling of direct energy requirements in mechanical machining processes. *J Clean Prod* 41:179–186
- Sen B, Mia M, Krolczyk G, Mandal UK, Mondal SP (2019) Eco-friendly cutting fluids in minimum quantity lubrication assisted machining: a review on the perception of sustainable manufacturing. *Int J Precis Eng Manuf Technol* 1–32
- Varadarajan A, Philip P, Ramamoorthy B (2002) Investigations on hard turning with minimal cutting fluid application (HTMF) and its comparison with dry and wet turning. *Int J Mach Tools Manuf* 42(2):193–200
- Mia M, Gupta MK, Adolfo LJ, Carou D, Pimenov DY, Krolczyk G, Khan AM, Dhar NR (2019) Multi-objective optimization and life cycle assessment of eco-friendly cryogenic N<sub>2</sub> assisted turning of Ti-6Al-4 V. *J Clean Prod* 210:121–133
- Maruda RW, Krolczyk GM, Wojciechowski S, Zak K, Habrat W, Nieslony P (2018) Effects of extreme pressure and anti-wear additives on surface topography and tool wear during MQCL turning of AISI 1045 steel. *J Mech Sci Technol* 32(4):1585–1591
- Hao X, Cui W, Li L, Li H, Khan AM, He N (2018) Cutting performance of textured polycrystalline diamond tools with composite lyophilic/lyophobic wettabilities. *J Mater Process Technol* 260:1–8
- Xing Y, Deng J, Zhang K, Zhang G, Gao H (2014) Effect of femtosecond laser pretreatment on wear resistance of Al<sub>2</sub>O<sub>3</sub>/TiC ceramic tools in dry cutting. *Int J Refract Met Hard Mater* 43:291–301
- Kim DM, Bajpai V, Kim BH, Park HW (2015) Finite element modeling of hard turning process via a micro-textured tool. *Int J Adv Manuf Technol* 78:1393–1405
- Sawant MS, Jain NK, Palani IA (2018) Influence of dimple and spot-texturing of HSS cutting tool on machining of Ti-6Al-4 V. *J Mater Process Technol* 261:1–11
- Velchev S, Kolev I, Ivanov K, Gechevski S (2014) Empirical models for specific energy consumption and optimization of cutting parameters for minimizing energy consumption during turning. *J Clean Prod* 80:139–149
- Zhang H, Deng Z, Fu Y, Wan L, Liu W (2017) Optimization of process parameters for minimum energy consumption based on cutting specific energy consumption. *J Clean Prod* 166:1407–1414
- Mishra SK, Ghosh S, Aravindan S (2018) Characterization and machining performance of laser-textured chevron shaped tools coated with AlTiN and AlCrN coatings. *Surf Coat Technol* 334:344–356
- Zhang K, Deng J, Xing Y, Li S, Gao H (2015) Effect of microscale texture on cutting performance of WC/Co-based TiAlN coated tools under different lubrication conditions. *Appl Surf Sci* 326:107–118
- Xie J, Luo MJ, He JL, Liu XR, Tan TW (2012) Micro-grinding of micro-groove array on tool rake surface for dry cutting of titanium alloy. *Int J Precis Eng Manuf* 13:1845–1852
- Sasi R, Kanmani Subbu S, Palani IA (2017) Performance of laser surface textured high speed steel cutting tool in machining of Al7075-T6 aerospace alloy. *Surf Coat Technol* 313:337–346
- Liu G, Huang C, Su R, Tuğrul Ö, Liu Y, Xu L (2019) 3D FEM simulation of the turning process of stainless steel 17-4PH with differently texturized cutting tools. *Int J Mech Sci* 155:417–429
- Kawasegi N, Sugimori H, Morimoto H, Morita N, Hori I (2009) Development of cutting tools with nanoscale and nanoscale textures to improve frictional behavior. *Precis Eng* 33:248–254
- Kummel J, Braun D, Gibmeier J, Schneider J, Greiner C, Schulze V, Wanner A (2015) Study on micro texturing of uncoated cemented carbide cutting tools for wear improvement and built-up edge stabilisation. *J Mater Process Technol* 215:62–70
- Xing Y, Deng J, Wu Z, Liu L, Huang P, Jiao A (2018) Analysis of tool-chip interface characteristics of self-lubricating tools with nanotextures and WS<sub>2</sub>/Zr coatings in dry cutting. *Int J Adv Manuf Technol* 97(5-8):1637–1647
- Li Y, Deng J, Chai Y, Fan W (2016) Surface textures on cemented carbide cutting tools by micro EDM assisted with high-frequency vibration. *Int J Adv Manuf Technol* 82:2157–2165
- Koshy P, Tovey J (2011) Performance of electrical discharge textured cutting tools. *CIRP Ann Manuf Technol* 60:153–156
- Kawasegi N, Ozaki K, Morita N, Nishimura K, Yamaguchi M (2017) Development and machining performance of a textured diamond cutting tool fabricated with a focused ion beam and heat treatment. *Precis Eng* 47:311–320
- Arulkirubakaran D, Senthilkumar V, Kumawat V (2016) Effect of micro-textured tools on machining of Ti-6Al-4 V alloy: an experimental and numerical approach. D, Arulkirubakaran, V, et al. Effect of micro-textured tools on machining of Ti-6Al-4 V alloy: an experimental and numerical approach[J]. *Int J Refract Met Hard Mater* 54:165–177
- Patel K, Liu G, Shah SR, Özel T (2020) Effect of micro-textured tool parameters on forces, stresses, wear rate, and variable friction in titanium alloy machining. *J Manuf Sci Eng* 142(021007):1–17
- Haddag B, Makich H, Nouari M, Dhers J (2014) Tribological behaviour and tool wear analyses in rough turning of large-scale parts of nuclear power plants using grooved coated insert. *Tribol Int* 80:58–70
- Haddag B, Nouari M, Barlier C, Dhers J (2014) Experimental and numerical analyses of the tool wear in rough turning of large dimensions components of nuclear power plants. *Wear* 312(1-2):40–50
- Xing Y, Deng J, Zhao J, Zhang G, Zhang K (2014) Cutting performance and wear mechanism of nanoscale and microscale textured Al<sub>2</sub>O<sub>3</sub>/TiC ceramic tools in dry cutting of hardened steel. *Int J Refract Met Hard Mater* 43:46–58
- Özel T, Altan T (2000) Determination of workpiece flow stress and friction at the chip-tool contact for high-speed cutting. *Int J Mach Tools Manuf* 40:133–152

**Publisher's note** Springer Nature remains neutral with regard to jurisdictional claims in published maps and institutional affiliations.